Study of reactor based anti-neutrinos

Mr. Yash Palan

Physics Department, IISER Bhopal,

Dr. P. K. Netrakanti

Nuclear Physics Division, Bhabha Atomic Research Center

Table of Contents

Source

Study of reactor based anti-neutrinos

Mr. Yash Palan

Physics Department, IISER Bhopal,

Dr. P. K. Netrakanti

Nuclear Physics Division, Bhabha Atomic Research Center

Abstract

The Standard Model (SM) in physics describes the physical laws and interactions of the atomic and subatomic particles. Neutrino is one such particle which deviated from the SM predictions. Experimental observation of neutrino oscillation and mass are such phenomenon which is not predicted by SM. Hence, Neutrinos become a frontier area for new research for new research. Nuclear reactors are man-made and copious source for anti-neutrino production. Nuclear reactors derive their power from fission processes. Each fission process produces 6 electron anti-neutrinos. The detection of these anti-neutrinos takes place via the process of Inverse Beta Decay (IBD). The energy of the detected anti-neutrinos ranges between 1.8MeV and 8.0MeV.

In the present work, we calculate the yield of the reactor anti-neutrinos which can be measeured by the process of the IBD. Four isotopes namely, U235, U238, Pu241, Pu239, comprise 99% of the reactor fuel. We check the dependence of the anti-neutrino yield on fuel composition by varying the fission fraction of these 4 isotopes. The products of the IBD are the positron and neutron. We then calculate the energy distribution of the positron and neutron as a function of energy of the produced anti-neutrinos.

The detection of anti-neutrinos in experiments, via IBD process, uses ~1 ton plastic or liquid based scintillator detectors. We characterize one such plastic scintillator bar of dimension 10cm x 10cm x 100cm for the calibration of energy, time and position resolution. We also study the response of gamma radiation from standard radioactive sources using an $CeBr_3$, inorganic scintillator based detector.

Keywords: standard model, inverse beta decay, plastic scintillator

Abbreviations

Abbreviations

Abbreviation	Full Form
SM	Standard Model
IBD	Inverse Beta Decay
PS	Plastic Scintllator
PMTs	Photo Multiplier tubes
AN	Anti Neutrino
ADC	Analog to Digital Converter
U	Uranium
Pu	Plutonium
e^-	Electron

1 Introduction

1.1 Background

The Standard Model (SM) of Physics is a theoretical framework in Physics which is used to describe the behavior of particles at the subatomic and atomic scales. The importance of the SM lies in the fact that it combines three of the 4 fundamental forces of nature, namely, the electromagnetic, weak and strong force. Also, most of the predictions from SM have been measured and verified experimentally.

Just like the atomic model, the SM states that all particles are made up elementary particles called quarks and leptons. For e.g. the proton and neutron each made up of 3 quarks. The interactions of these quarks and leptons are facilitated by force carries namely, photons, gluons, W and Z bosons. The most recent particle which was discovered in experiments at LHC, the Higgs Boson, provided the fundamental nature of the electro weak symmetry breaking, causing these partons to acquire mass.

In the SM, there are 6 quarks: namely up (u), down (d), charm (c), strange (s), bottom (b) and top (t). Along with these quarks, there are 6 leptons namely electron, muon, tau, and 3 neutrinos as well as the 5 force carriers mentioned before.

Figure 1 depicts the elementary particles of the Standard Model of Physics.

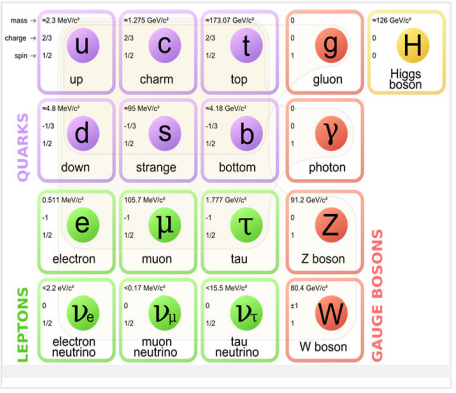

Fig 1 Standard Model of Physics

Recent experiments like the Solar neutrino Experiment (SNO) showed a deficit in the flux of electron type neutrinos in comparison to what was predicted by the SM. Though, when all 3 types of neutrinos were considered, the predictions matched. This gave rise to the theory of neutrino oscillation, which is a phenomenon not described by the SM.

The phenomenon of neutrino oscillations caused a great interest in the current generation of neutrino experiments. The search included determination of neutrino masses and the oscillation angles θ_{13}, θ_{23} and θ_{12}.

Nuclear reactors are a copious source of electron antineutrinos emanating from the fission of nuclear fuel composition. Many recent experiments, performed for the search of θ_{13}, θ_{23} and θ_{12}, have used antineutrinos generated from Nuclear Reactors. The most common technique used for detection the electron type antineutrino is the Inverse Beta Decay (IBD). Hence, it becomes extremely important to study the IBD process in conjunction with the antineutrinos generated by a Nuclear Reactor.

In the IBD, an electron antineutrino interacts with a proton to give out a neutron and a positron. Most of the energy of the antineutrino is carried away by the positron. Hence, a measurement of the positron energy allows for a measurement of the energy of the incident antineutrino. This is most commonly done by the use of large scale detectors made of organic scintillators coupled with Photo Multiplier Tubes (PMTs) readout system.

Positron loses energy via specific ionization in the scintillator medium and comes to rest. At rest, it annihilates with an electron to give two photons of energy 0.511 MeV , which

are detected by the use of PMTs. This signal of positron energy loss with two annihilation photons constitutes the prompt signal.

Neutron, on the other hand, thermalizes in the medium and is captured either on Hydrogen (H), or a doping element, e.g. Gadolinium (Gd), which has a very large thermal neutron capture cross-section. The capture of thermal neutron on Gd excites the Gd nucleus. During de-excitation the nucleus emits a cascade of gamma rays having a total energy of 8 MeV. This comprises the delayed signal.

Hence, for an experiment to be successful in detection of antineutrinos via IBD, requires the accurate measurement of prompt and delayed signals.

Studying the response of organic scintillators for gamma and neutrons becomes important for the classification of the IBD events.

1.2 Objectives of the research

In this study, we simulate the process of anti neutrino generation from a reactor along with the IBD phenomenon that take place inside an organic scintillator detector. We try to understand the spectra of anti-neutrinos generated from a nuclear reactor and its dependence on the fuel composition. We further generate Monte-Carlo based energy spectrum of the positrons and neutrons resulted from the IBD of anti-neutrinos.

In the second part, we study the response an inorganic scintillator detector namely Cerium Bromide ($CeBr_3$), and an organic scintillator: Plastic Scintillator (PS). Energy calibration for the both the scintillator detectors is done and their energy resolution is studied by the use of standard radioactive sources like ^{60}Co, ^{22}Na, and ^{137}Cs.

2 Literature Survey

2.1 Inverse Beta Decay (IBD)

The most common method of inducing fission in a nuclear reactor is by the use of thermal neutrons. Energy of these neutrons is just enough so that it can cross the nuclear potential barrier and enter the nucleus. This causes a transition of the nucleus into an excited state. The nucleus then splits into 2 daughter nuclei, releasing multiple neutrons. These daughter nuclei undergo subsequent β decays to attain a stable configuration. Each β decay releases one electron type antineutrino. The IBD process is used for the detection these antineutrinos.

The Inverse beta decay process refers to the conversion of a proton and an electron antineutrino to a neutron and a positron**.**

From now on whenever we refer to an Anti-Neutrino (AN), we mean an electron antineutrino (unless mentioned otherwise).

The equation for the IBD is given as

$$p^+ + \bar{\nu}_e \text{ - - - > } n + e^+$$

where e^+ refers to a Positron, $\overline{\nu}_e$ refers to an AN, p^+ refers to a proton and n refers to a neutron

The Feynman diagram for the above process is given as

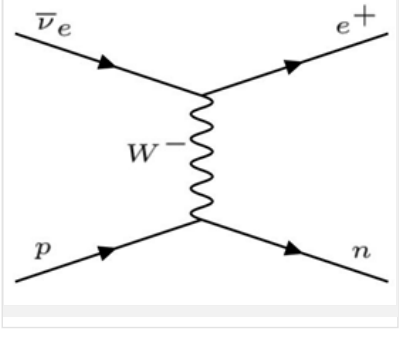

Fig 2 Feynman Diagram for the IBD process. In the IBD process, an antineutrino and a proton interacting by exchange of a W- boson creates a positron and neutron.

The u quark in proton changes to a d quark by the exchange of a W+ boson with an AN. The acceptance of W+ boson by the AN causes it to convert to a positron.

The process is mediated by the Weak Nuclear Force (as depicted by the exchange of the W+ boson).

This technique of AN detection has been used in many experiments like Double Chooz, RENO, Daya Bay, etc.

Heuristically, the AN must have sufficient energy to be able to convert the proton to a neutron, and also "create" a positron.

The minimum energy of the antineutrino to be detected via IBD should be ~$M_n + M_e - M_p$

= (939.57 +0.511 – 938.28) MeV = 1.801 MeV

where M_n=mass of neutron , M_p = mass of proton, M_e= mass of electron .

Hence, only those ANs can be observed which have energy greater than 1.8 MeV. The range of the reactor ANs measured by IBD is from 1.8MeV – 8.0 MeV. In our analysis, the AN energy range selected is from 2.0 MeV- 8.0 MeV.

2.2 **Reactor Flux Model**

A nuclear reactor is powered by the process of nuclear fission, which is the breaking up of heavier nuclei into lighter nuclei to produce energy. The primary process by which this happens is called Beta Decay. In one beta decay, one neutron is converted to a proton, electron and an AN. The energy of AN emitted from one single beta decay lies in the range of 1-8 MeV[1].

A single fission generally implies 6 beta decays. A typical power reactor has a power of ~3GW_{th} and produces ~200MeV of energy in each fission process. The typical yield of ANs at equilibrium is ~6x 10^{20} ANs per core per second [1].

There are two main ways of determination of the AN spectra from a Nuclear Reactor:-

1. Summation Method:-

a. This uses the cumulative fission yield and the branching ratios for all beta decay branches and a normalized Shape function to determine the no. of AN generated for a given AN energy.

b. Disadvantages :

i. The Branching ratios are sometimes poorly known. This can cause high amounts of errors to creep into further calculations.

ii. All the decays are not of the allowed type. So, it is essential to only include the ones which are allowed. This is a very hard task [1].

2. Experimentally determined electron Spectrum

a. The e^- spectrum was first measured at ILL Grenoble for the fission of ^{235}U, ^{238}U, ^{239}Pu, ^{241}Pu. The above was then transformed into the AN spectra, using the fact that 2 leptons share the energy of each beta decay branch. The conversion is done assuming that the e^- spectrum is known precisely [1].

Earlier models generally used the 1st technique, though now, the latter is more preferred [1].

But, recent experiments have also raised the question that whether the electron spectrum was measured precisely. This question arose because of the presence of small changes in the experimental AN spectra when compared to the theoretical predictions of the SM [1].

2.3 **Detector Calibration**

Scintillation refers to a flash of visible or UV light emitted by fluorescence in a phosphor when struck by a charged particle or high energy photon.

Scintillation detectors are one of the most widely used methods for detection of photons. An ideal scintillator must have the following properties:-

1. Should convert kinetic energy of charged particles/photons into detectable light.

2. Conversion should be linear.

3. The medium should be transparent to the wavelength of its own emission.

4. The decay time of the induced luminescence should be short.

5. The index of refraction of the material should be ~1.5, so that coupling with a PMT is easier [2].

Inorganic Scintillators Mechanism

In solids, e^- are available only in discrete bands of energy. There are 2 such bands: the Valence band and the conduction band. The Valence band contains all the e^- in the ground state, while the conduction band represents electrons which have sufficient energy to be free enough to migrate through the crystal. In between the 2 bands, is a region called a Forbidden region, where e^- can never be found in a pure crystal [2].

Absorption of energy can result in the elevation of an e^- from the valence band to the conduction band. In a pure crystal, the de-excitation of the e^- with an emission of a photon is very less probable [2].

To increase the probability of the above process, the pure crystal is doped with impurities called Activators. These Activators generate energy levels inside the Forbidden region, through which the e^- can de-excite. Such centers are called Recombination Centers [2].

When a charged particle (or photon) passes through a detection medium, it deposits energy to an e^-, and forms an electron-hole pair. The e^- and hole drift through the crystal until they reach a recombination center, where the e^- de-excites and a photon is emitted. This is far more feasible as the energy gap at the recombination center is reduced in comparison to that of the pure crystal [2].

Also, since the energy of the emitted photon is lower than the band gap, the detector is transparent to its own emission wavelength [2].

3 Methodology

3.1 Concepts

3.1.1 Reactor Antineutrino Flux

About 99% of a Reactor's fuel consists of ^{235}U, ^{238}U, ^{239}Pu and ^{241}Pu.

The total reactor flux φ can be written as [3]

$$f(E_v) = \sum_i a_i exp(\sum_{j=0}^{5} b_{ij} E_v^j) \quad (1)$$

Where a_i is the isotope fraction in the fuel, is energy of anti neutrino ,b_{ij} s are the constant terms used to fit the neutrino spectrum

(Table 1)[7] and $i \in \{ {}_{92}^{235}U, {}_{92}^{238}U, {}_{94}^{239}Pu, {}_{94}^{241}Pu \}$.

Table 1

Element	b0	b1	b2	b3	b4	b5
U235	3.217	-3.111	1.395	-0.3690	0.04445	-0.002053
U238	0.4833	0.1927	-0.1283	-6.762×10^{-03}	2.233×10^{-3}	-1.536×10^{-4}
Pu239	6.413	-7.432	3.535	-8.82×10^{-1}	1.025×10^{-1}	-4.550×10^{-3}
Pu241	3.251	-3.204	1.428	-3.657×10^{-1}	4.254×10^{-2}	-1.896×10^{-3}

The Thermal power of the reactor is given in terms of the fission fractions as

$$P_{th} = \sum_i a_i p_i$$

where p_i= the thermal energy released in one fission by isotope i [4].

Using the equation 1, we can simulate the AN flux for a reactor having a certain fuel composition.

3.1.2 Inverse beta Decay Cross Section

The IBD cross section is given by the following equation [5]

$$\sigma_{tot} = \sigma^0 * (f^2 + 3g^2) E_e p_e \quad (2)$$

$$\sigma_{tot} = 0.0952 * \frac{E_e p_e}{(1MeV)^2} * 10^{-42} cm^2$$

where E_e is the energy of the positron and pe is the momentum of the positron. To first order, E_e is given by

$$E_e = E_v - (m_n - m_p)$$

m_n = Rest mass of neutron

m_p = Rest mass of proton

E_v = Energy of antineutrino

3.1.3 Antineutrino Spectra

The no. of antineutrinos N is given by

$$N = f(E_v) * \sigma_{tot} (E_v) \quad (3)$$

3.1.4 Inverse Beta Decay

We now derive the relations between the antineutrino energy and the positron energy for a 1D case.

Let E_v,E_e, $E_n$and E_p denote the energy of AN, positron, neutron and proton respectively.

Let p_v, $p_e$and $p_n$denote the momentum of the AN, positron and neutron respectively.

Rest mass of an AN is assumed to be 0 MeV. Hence,

$$p_v * c = E_v \quad (4)$$

Assuming that the target proton has 0 momentum, and then applying momentum conservation we get

$$p_v = p_e + p_n$$

From equation 4, we get

$$p_n = p_v - p_e = \frac{E_v}{c} - p_e \quad (5)$$

Applying energy conservation

$$E_v + m_p c^2 = E_e + E_n \quad (6)$$

Replacing $m_i c^2 = C_i$, where $i \in \{p, n, v, e\}$

$$E_n = E_v + C_p - E_e$$

$$p_n^2 c^2 + C_n^2 = (E_v + C_p - E_e)^2$$

Using equation 5

$$2E_e(E_v - C_p) = C_p(2E_v + C_p) + C_e^2 - C_n^2 + 2E_v p_e c$$

Substituting $b = 2(E_v - C_p)$, $a = 2E_v$ and $k = C_p(2E_v + C_p) + C_e^2 - C_n^2$

$$E_e b = k + a p_e c$$

$$(b^2 - a^2) E_e^2 - 2bkE_e + k^2 + a^2 C_e^2 = 0$$

Using the quadratic formula, we get

$$E_e = \frac{(bk + \sqrt{D})}{(b^2 - a^2)} \quad (7)$$

where $D = b^2 k^2 - (b^2 - a^2)(k^2 + a^2 C_e^2)$

Equation 7 gives us the energy of positron in terms of the energy of the AN.

Let KE_i denote the Kinetic energy of particle i, where $i \in \{p, n, v, e\}$.

Then $KE_i = E_i - m_i c^2$

3.1.5 Klein-Nishina Formula [3]

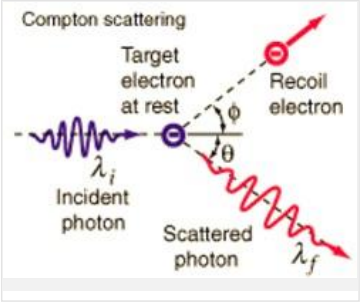

Fig 3 Compton Scattering

Compton scattering refers to the scattering of photons by charged particles, generally e^-. This is an example of inelastic scattering as the incoming photon and outgoing photon have different wavelength (and hence different momenta). The shift in wavelength is known as Compton Shift. In low Z materials (like PS), when the incident photon's energy is in the range of 1 MeV – 10 MeV, Compton Scattering is the dominant process (in comparison to pair production and photoelectric effect) [6].

The Compton Scattering process is described in the Fig3.

Let $v = c/\lambda_i$ and $v' = c/\lambda_f$.

Then,

$$hv' = \frac{hv}{(1 + \gamma(1 - cos\theta))} \quad (8)$$

Where $\gamma = h\nu / (m_e c^2)$

Let T denote the energy of the scattered e-, then

$$T = h\nu' - h\nu \quad (9)$$

The Klein-Nishina formula is a formula that gives the cross section for the process of Compton Scattering. The equation is as follows [6]

$$\frac{d\sigma}{d\Omega} = \frac{r_e^2}{2} * \frac{1}{[\,1 + \gamma(1 - \cos\theta)\,]^2} * 1 + \cos^2\theta + \frac{\gamma^2(1 - \cos\theta)^2}{1 + \gamma(1 - \cos\theta)} \quad (10)$$

So, we get,

$$\frac{d\sigma}{dT} = \left(\frac{\pi r_e^2}{m_e c^2 \gamma^2}\right)\left(2 + \frac{s^2}{(1 - s^2)\gamma^2} + \frac{s}{(1 - s)(s - 2/\gamma)}\right) \quad (11)$$

Where $s = T / h\nu$.

3.2 **Methods**

1. Inverse beta Decay Simulation

· The IBD simulation was carried out by the use of C++ and ROOT (CERN based software).

· The flux and IBD cross section functions were created. These were used for the calculation of the AN spectra.

· Then, using the random no. generator (generated using the AN Spectra), antineutrinos were created and the resultant positron and neutron energies were calculated.

· The total sample size used was 100000. The results of the above experiments were then filled in a histogram.

2. Calibration of detector with standard sources:-

· Data was taken using standard sources like ^{137}Cs, ^{22}Na, ^{60}Co using a $CeBr_3$ and PS detector. The electrical signal was taken from a PMT and then sent to a digitizer, which stored the resultant ROOT file. The digitizer stores the data in terms of channel numbers. The resolution of the Analog to Digital Converter (ADC) is 32k bytes.

· For Calibration of CeBr3, the photo-peaks were used. A Gaussian fit was performed on the photo-peaks, and the mean value was noted. This was then used to plot the Calibration curve for CeBr3.

· A linear fit was performed to fit the points obtained. This gives the calibration curve for the detector.

· The calibration curve was used to convert the data form channel no. to energy.

· A Gaussian fit was again performed on the photo-peaks, the mean and sigma recorded. These were used for obtaining the energy resolution curve for the detector.

4 Results and Discussion

4.1 Inverse beta Decay Simulation

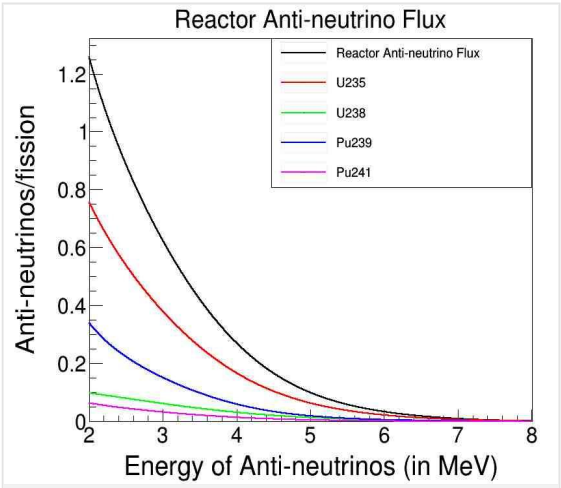

Fig 4 Flux of anti-neutrinos for different isotopes of U and Pu. The total integrated flux from combination of all the isotopes is shown in black curve.

Figure 4 depicts the no. of antineutrinos generated per fission for the given reactor composition. It also depicts the contributions of the individual isotopes in the total flux.

The fuel used for the above analysis is composed of 57% ^{235}U, 7% ^{238}U, 30% ^{239}Pu, 5% ^{241}Pu. This is the fuel composition used at Daya Bay.

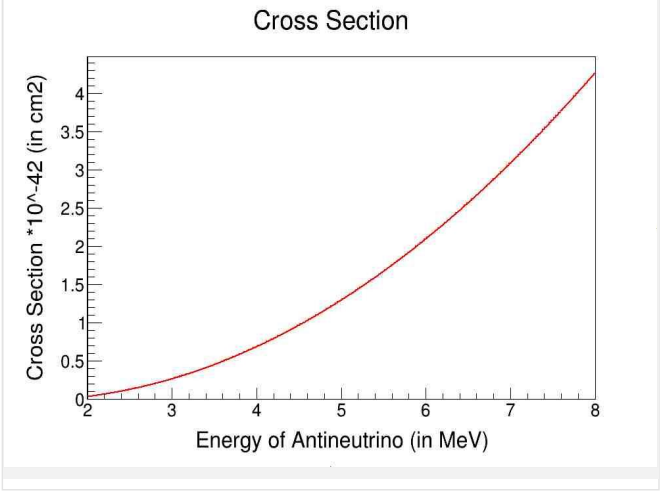

Fig 5 AN cross section for IBD process as a function of the AN energy

The IBD cross section increases with an increase in anti-neutrino energy as shown in Fig5.

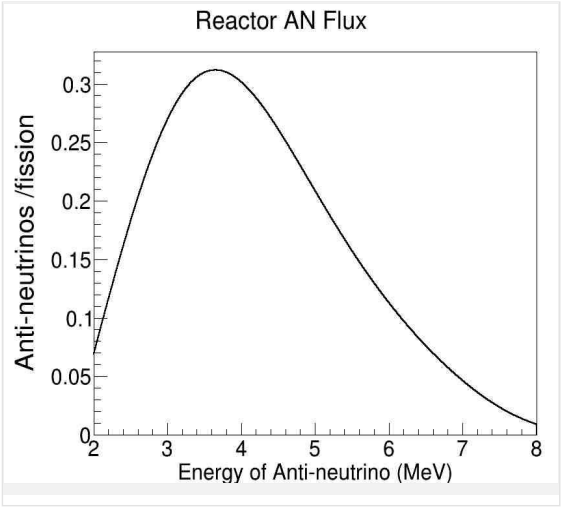

Fig 6 Reactor AN spectra for the IBD process.

Convolution of the flux (fig 4) with cross-section (fig 5) gives the Reactor AN flux, as shown in fig 6.

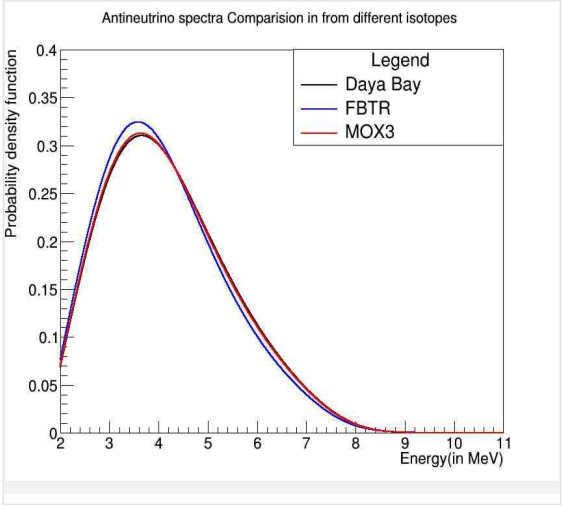

Fig 7 AN spectra for different reactor fuels.

Figure 7 depicts the AN spectra generated for different types of reactor fuels. The fuel compositions used for comparison were ones used in Daya Bay, MOX3 fuel and FBTR.

Figure 7 used the fuel composition used by Daya Bay, MOX3 fuel and FBTR and compares the three. MOX3 and Daya Bay fuel compositions give approximately the same antineutrino spectra. On the other hand, the FBTR has an observable difference in the anti neutrino spectra.

The fuel composition for FBTR is 0.93% ^{235}U, 10% ^{238}U, 71% ^{239}Pu, 11% ^{241}Pu while that for the MOX3 is 51% ^{235}U, 6.6% ^{238}U, 39% ^{239}Pu, 3.1% ^{241}Pu. Clearly, FBTR fuel contains a larger fraction of Plutonium in comparison to the other two types of fuels.

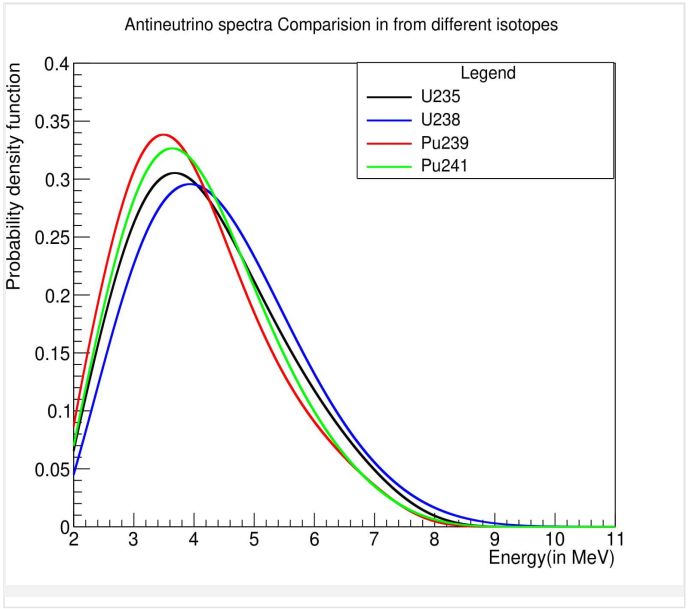

Fig 8 AN spectra for ^{235}U, ^{238}U, ^{239}Pu and ^{241}Pu

Figure 8 compares the antineutrino spectra generated by a hypothetical reactor if only one of the isotopes were used as fuel.

We observe that for ^{239}Pu, the average energy of the anti neutrinos generated is lowest in comparison to the other 3 isotopes. Hence, the decrease in average energy for the FBTR fuel, in comparison to the other 2 fuels, is mainly due to the presence of greater fraction of ^{239}Pu.

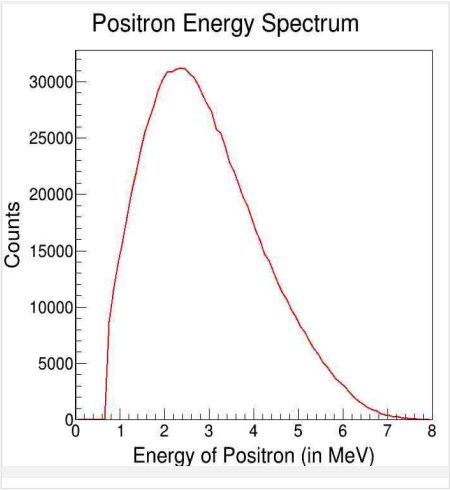

Fig 9 Energy spectrum for the positron generated by the IBD process. The spectrum was generated by a Monte Carlo analysis of the IBD.

Figure 9 was obtained by a Monte Carlo analysis of the IBD. About 100000 antineutrinos were generated randomly, weighted by the spectrum shown in fig 3. The energy of the positrons generated by the IBD process was calculated and filed into a histogram. Figure 9 clearly depicts the fact that maximum of the energy of the anti neutrino is carried by positron. Hence, a measurement of the positron energy would result in the measurement of the energy of the antineutrino.

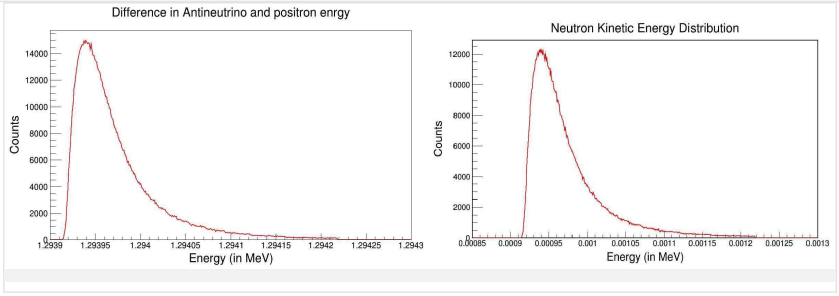

Fig 10 (Left) Spectrum for the difference between the AN energy and positron energy. (Right) Distribution of kinetic energy of neutron generated as a result of the IBD process.

We see a very sharp peak at 1.29395 MeV. The mass difference between the neutron and the proton is 1.29 MeV. Hence, the neutron gains some Kinetic energy as a result of the interaction. Notice that the energy maxima in Fig 10 (right) is at 0.95 keV. Hence, the kinetic energy of the neutron is extremely small in comparison to that of the positron and hence can be neglected.

4.2 Calibration

Yet, the neutron capture delay signal combined with the positron annihilation prompt signal is a very strong coincidence signal, which is used to reduce background in AN detection. That is why neutron capture is an integral part of the AN detection process, despite it taking away so less energy of the incident AN.

Plastic scintillators (PS) are solutions of organic scintillators in solid plastic solvents. Some examples of PS are polyvinyltoulene and polymethylmethacrylate. These are one of the most widely used organic scintillator detectors because of the low decay time resulting in an extremely fast signal. The drawback of these types of scintillator detectors is the low resolution and the absence of photo-peaks [2].

$CeBr_3$ is a relatively fast inorganic detector having high resolution. The resolution of CeBr3 is 4% full width half maxima at 662 keV. The decay, when measured in the visible band, is an exponential with a decay time of 27ns. The drawback of this is that the total light yield is very low [2].

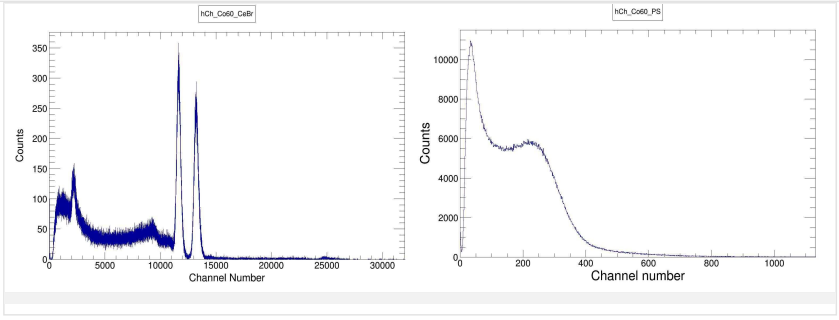

Fig 11 Gamma ray spectrum for ^{60}Co as measured from $CeBr_3$ (left) and PS (right).

Figure 11 depicts the gamma ray spectrum for ^{60}Co as measured by both the detectors. In $CeBr_3$(as shown in left), both the photo-peaks and Compton edge are sharply defined. This is in contrast to the PS, where no photo-peak is observed. The Compton edge is the only observable feature in the spectra detected by the PS.

For $CeBr_3$, photo-peaks have been used for calibration. In PS, Compton edge is used for calibration purposes.

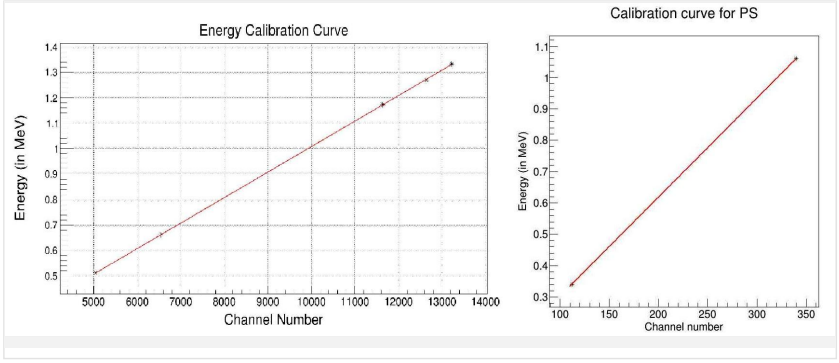

Fig 12 Calibration curve for $CeBr_3$ (left) and PS (right)

Figure 12 shows the calibration curve obtained for CeBr3. The sources used for obtaining the points are ^{60}Co, ^{137}Cs and ^{21}Na. Figure 13 shows the calibrated spectrum for ^{60}Co.

Calibration for PS is done using the Compton edges of the 0.511MeV and 1.27 MeV transitions in ^{21}Na. Within this energy range, the calibration curve is linear for both the detectors.

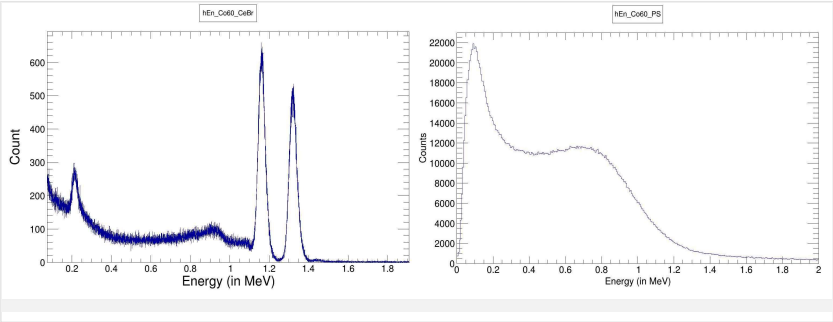

Fig 13 Energy spectrum for ^{60}Co measured by $CeBr_3$ detector (left) and PS detector(right).

Figure 13 depicts the energy spectrum of ^{60}Co as measured by both the detectors. $CeBr_3$ is a high detector having high atomic number (Z) due to which both photoelectric effect and Compton Scattering are dominant processes. So, we observe 2 photo-peaks: one with energy 1.33 MeV and the other with energy 1.17 MeV. Also, compton edge corresponding to the 2 photo-peaks can also be observed, along with one backscatter peak (~0.2 MeV) from surrounding material.

On the other hand, PS has a low Z value and hence Compton scattering is the only dominant process within this energy range. Also, only one Compton plateau is observable. This is because of the poorer energy resolution of the PS. Due to the poorer energy resolution, one may expect a shift in the Compton edge. Hence, the maxima, which is observed in the spectrum, is not the true Compton edge, as would be expected in the theoretical case. To estimate the shift of the maxima due to energy resolution, we performed a simulation where the energy resolution is convoluted as a parameter to the quantum mechanical calculated Klien-Nishina formula. This shift is shown qualitatively below in Fig 14 for different energy resolution for incident photon energy of 0.662 MeV. The true Compton edge corresponding to the above energy is ~0.477 MeV.

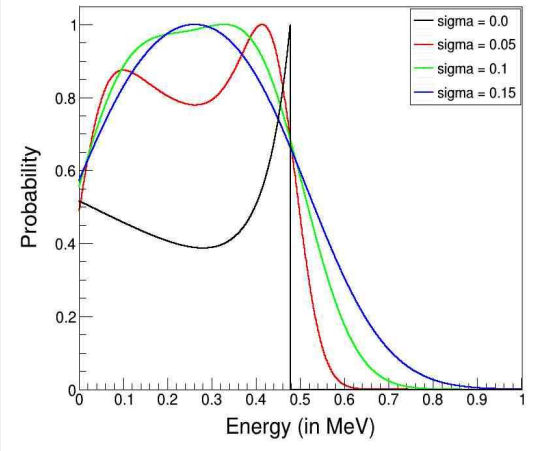

Fig 14 Figure 14: Detector response for varying energy resolutions. The graphs are generated by convoluting the Gaussian response of a detector with the theoretical Klein-Nishina function.

Figure 14 clearly illustrates the fact that the maxima of the convoluted curve shifts to the left of the theoretical Compton edge (i.e. 0.477 MeV) as the sigma increases.

The calibration of the PS was done taking this shift into account.

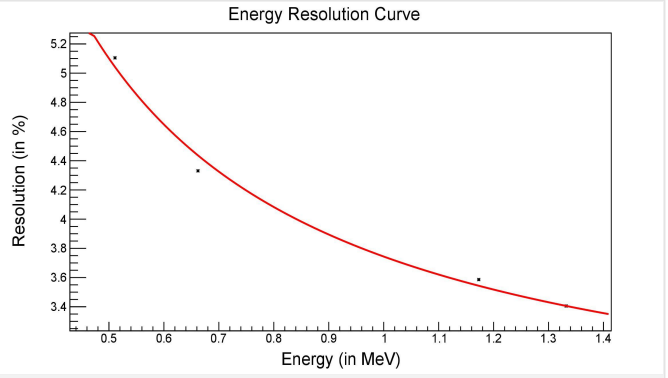

Fig 15 Energy Resolution of $CeBr_3$ as a function of energy.

The energy resolution for $CeBr_3$ is plotted as a function of energy in fig. 15. The function used for fitting the data points is

$$f(E) = a^2 + \frac{b^2}{\sqrt{E}} + \frac{c^2}{E} \quad (12)$$

where a^2= Constant Term, $\frac{b^2}{\sqrt{E}}$ = Stochastic term, $\frac{c^2}{E}$= Noise term

5 Conclusion

Observation of reactor AN flux can also be used as a method for remote monitoring the reactor. This can be done because of the fact that while the reactor is running, the fuel composition changes and this causes a change in the reactor AN spectrum, which can be used to figure out the final fuel content and hence the power of the reactor remotely and in a non intrusive way. Further scope of this work would be to include the radiative, weak magnetic and nucleus recoil correction in the IBD cross section formula.

We also characterized Plastic Scintillator and CeBr3 detectors for use in antineutrino measurements for signal and background events.

6 References

[1] Vogel P., Wen L. J., Zhang C., Nature Communications 6, (2015) 6935.

[2] Radiation Detection and Measurement by Glenn F. Knoll.

[3] Behera, S.P., Mishra, D.K. & Pant, L.M., Eur. Phys. J. C (2019) 79:86.

[4] Christensen E., Huber P., Jafke P., arXiv:1312.1959v2.

[5] Vogel P., Beacom J. F., Phys.Rev. D60 (1999) 053003.

[6] Techniques for nuclear and particle physics experiments by William R. Leo.

[7] Huber, P Phys. Rev. C 84 (2011) 024617.

7 Acknowledgements

I would like to thank the Indian Academy of Sciences for providing me an opportunity to learn more about research, in the form of this summer research fellowship.

I am extremely grateful to my Guide, Dr. P. K. Netrakanti, for giving me a chance to explore the field of High Energy Physics and allowing me to see the wonders of this field, as well as its challenges and its amazing possibilities. I express my gratitude to all in the NPD division, BARC for solving whatever queries I has. I would like to thank the PhD students at NPD,BARC and my fellow interns for making this a memorable experience.

Last, I express my gratitude to BARC for providing me this wonderful opportunity. Also, a big thanks to Authorcafe support staff for all the support it has provided whenever I had an issue during the writing process.

Source

1. Fig 1: https://en.wikipedia.org/wiki/Standard_Model
2. Fig 2: https://www.researchgate.net/publication/315458901_Neutrino_Physics_in_Present_and_Future_Kamioka_Water-Cherenkov_Detectors_with_Neutron_Tagging/figures?lo=1&utm_source=google&utm_medium=organic
3. Fig 3: http://hyperphysics.phy-astr.gsu.edu